2-[^{18}F]Fluoropropionic Acid PET Imaging of Doxorubicin-induced Cardiotoxicity

Juan A. Azcona
Weill Cornell Medical College: Weill Cornell Medicine
Anja S. Wacker
Weill Cornell Medical College: Weill Cornell Medicine
Chul-Hee Lee
Weill Cornell Medical College: Weill Cornell Medicine
Edward K. Fung
Weill Cornell Medical College: Weill Cornell Medicine
Thomas M. Jeitner
Weill Cornell Medical College: Weill Cornell Medicine
Onorina L. Manzo
Weill Cornell Medical College: Weill Cornell Medicine
Annarita Di Lorenzo
Weill Cornell Medical College: Weill Cornell Medicine
John W. Babich
Weill Cornell Medical College: Weill Cornell Medicine
Alejandro Amor-Coarasa
Albert Einstein College of Medicine
James M. Kelly
jak2046@med.cornell.edu

Weill Cornell Medical College: Weill Cornell Medicine https://orcid.org/0000-0002-0525-0047

Research Article

Keywords: Doxorubicin, Cardiotoxicity, Positron Emission Tomography, Short-chain Fatty Acid, Fatty Acids, Metabolism, 2-[18F]Fluoropropionic Acid, Monocarboxylate, AZD3965

Posted Date: October 15th, 2024

DOI: https://doi.org/10.21203/rs.3.rs-4876095/v1

Abstract

Purpose

Treatment of pediatric cancers with doxorubicin is a common and predictable cause of cardiomyopathy. Early diagnosis of treatment-induced cardiotoxicity and intervention are major determinants for the prevention of advanced disease. The onset of cardiomyopathies is often accompanied by profound changes in lipid metabolism, including an enhanced uptake of short-chain fatty acids (SCFA). Therefore, we explored the utility of 2-[^{18}F]fluoropropionic acid ([^{18}F]FPA), an SCFA analog, as an imaging biomarker of cardiac injury in mice exposed to doxorubicin. *Procedures*: Cardiotoxicity and cardiac dysfunction were induced in mice by an 8-dose regimen of doxorubicin (cumulative dose 24 mg/kg) administered over 14 days. The effects of doxorubicin exposure were assessed by measurement of heart weights, left ventricular ejection fractions, and blood cardiac troponin levels. Whole body and cardiac [^{18}F]FPA uptakes were determined by PET and tissue gamma counting in the presence or absence of AZD3965, a pharmacological inhibitor of monocarboxylate transporter 1 (MCT1). Radiation absorbed doses were estimated using tissue time-activity concentrations.

Results

Significantly higher cardiac [^{18}F]FPA uptake was observed in doxorubicin-treated animals. This uptake remained constant from 30 min to 120 min post-injection. Pharmacological inhibition of MCT1-mediated transport by AZD3965 selectively decreased the uptake of [^{18}F]FPA in tissues other than the heart. Co-administration of [^{18}F]FPA and AZD3965 enhanced the imaging contrast of the diseased heart while reducing overall exposure to radioactivity.

Conclusions

[^{18}F]FPA, especially when co-administered with AZD3965, is a new tool for imaging changes in fatty acid metabolism occurring in response to doxorubicin-induced cardiomyopathy by PET.

Introduction

A significant number of cardiovascular disease cases arise due to an earlier treatment of cancer[1]. The treatment of pediatric cancers with doxorubicin, while often successfully eliminating the cancer, leads to cardiac dysfunction later in life for up to 10% of cancer-free patients[2,3]. Timely diagnosis of this cardiotoxicity can facilitate disease-mitigating treatment and prevent onset of severe dysfunction or even failure. Thus, there is an urgent need for novel methods to detect incipient injury to the heart in cancer patients undergoing treatment.

Long-chain fatty acids (LCFA) act as the primary energy source for the heart, with glucose, lactate, short-chain fatty acids (SCFA), and ketone bodies also serving as metabolic substrates. Aberrant LCFA metabolism is a hallmark of cardiac disease, such as that induced by doxorubicin treatment[4]. This metabolic dysfunction results in the compensatory uptake and oxidation of SCFA[5–7], such as propionic acid. Recently, 2-[^{18}F]fluoropropionic acid ([^{18}F]FPA) was developed to identify explanted prostate and liver cancers in mice[8–11] by positron emission tomography (PET). Subsequent first-in-human [^{18}F]FPA PET imaging of a prostate cancer patient included images of the heart where the delineation along the short and long axes confirm that [^{18}F]FPA is taken up by this tissue[12].

Despite the importance of SCFA oxidation to metabolically reprogrammed cardiomyocytes in the diseased heart, PET imaging approaches for targeting this pathway have not been pursued. We hypothesized that [^{18}F]FPA would be taken up to a greater extent by hearts exposed to doxorubicin in a manner that is distinguishable by PET. To test this hypothesis, we investigated [^{18}F]FPA PET as a modality for imaging overt cardiotoxicity caused by doxorubicin with a view towards applying this technique to imaging early-stage subclinical disease. Here, we report that the hearts of mice exposed to doxorubicin took up [^{18}F]FPA to a greater extent than the hearts of healthy mice. Furthermore, we developed an optimized imaging protocol for [^{18}F]FPA PET and showed that co-administration of the monocarboxylate transporter 1 (MCT1) inhibitor, AZD3965, increased the contrast between cardiac and non-cardiac tissues and significantly reduced the overall tissue radiation absorbed dose.

Materials and Methods

Full experimental details, including the radiosynthesis of [^{18}F]FPA, descriptions of imaging procedures, biodistribution experiments, dosimetry calculations, blood biomarker measurements, and cardiac acyl-CoA synthetase short chain (ACSS) family activity measurements, are available in the Electronic Supplementary Materials.

Synthesis of [^{18}F]FPA

The synthesis of [^{18}F]FPA was carried out according to published methods, with small modifications[13]. Briefly, racemic [^{18}F]FPA was synthesized in two steps from methyl-2-bromopropionate using no-carrier-added [^{18}F]fluoride. The radiotracer was obtained in activities of up to 1.5 GBq at end-of-synthesis and formulated for injection in saline. [^{18}F]FPA was obtained in 20–30% non-decay corrected yield and greater than 99% radiochemical purity.

Mouse Model of Doxorubicin-induced Cardiotoxicity

Ten-week-old male C57BL/6J mice (n = 22) were injected intraperitoneally with 8 x 3 mg/kg of doxorubicin over the course of two weeks, receiving a cumulative dose of 24 mg/kg. The respective

controls (*n* = 18) were injected with saline. All animal studies were approved by the Institutional Animal Care and Use Committee at Weill Cornell Medicine.

microPET/CT Imaging Studies

Mice (n = 9–11 per group) were injected intravenously with 9.25–11.1 MBq of [^{18}F]FPA in 100–150 µL saline containing either 5 mg/kg AZD3965 or DMSO (4–6 µL). A 60 min dynamic PET acquisition was performed beginning 30- or 60-min post-injection (p.i.) using the Siemens Inveon™ system. Cardiac uptake was determined by image-based quantification using the AMIDE software and expressed as a ratio of percent injected dose and tissue volume (%ID/cm^3).

Statistical Analyses

Data illustrations and analyses were performed using the GraphPad Prism 10 software. All data are expressed as means ± S.E.M.. Statistical tests performed include independent t-tests and two-way ANOVA. Tukey post hoc tests were used for multiple comparisons between all groups and Šídák post hoc tests were used for multiple comparisons between experimental groups and their respective controls. A *p*-value < 0.05 was considered to be statistically significant. All *n* values represent individual biological replicates.

Results

Fasting does not alter cardiac uptake of [^{18}F]FPA

2-Deoxy-2[^{18}F]fluoro-D-glucose ([^{18}F]FDG) PET is often preceded by a period of dietary fasting of at least 4–6 hours that is critical for some applications of cardiac diagnostic imaging[14]. We therefore assessed whether the cardiac and overall tissue uptake of [^{18}F]FPA is influenced by fasting. As shown in Fig. 1, fasting does not significantly affect the uptake of [^{18}F]FPA by tissues, although marginal decreases were seen in the brain and the gut.

AZD3965 improves image contrast for cardiac [^{18}F]FPA PET

The uptake of SCFA, such as [^{18}F]FPA, by the heart does not primarily rely on MCT1 as it does in other tissues[7,15,16]. We therefore reasoned that blocking the ingress of [^{18}F]FPA via MCT1 in non-cardiac tissues would improve contrast in the region of the heart and reduce whole body radiation absorbed dose. Indeed, AZD3965 increased the distinction between cardiac and extra-cardiac tissues (Fig. 2A). We treated mice with three concentrations of AZD3965 (0.05 mg/kg, 0.5 mg/kg, 5 mg/kg) and determined that a dose of 5 mg/kg almost completely suppressed [^{18}F]FPA uptake in extra-cardiac tissues without decreasing cardiac uptake. Based on time activity curves (TACs) of the hearts, livers, kidneys, and brains of mice injected with [^{18}F]FPA and 5 mg/kg AZD3965 or [^{18}F]FPA alone, we determined that cardiac uptake of [^{18}F]FPA remains essentially unchanged between 30 and 90 min p.i. (Fig. 2B) in both groups. A

similar trend was evident in liver and brain, although uptake in these tissues was significantly lower in the AZD3965 group than the DMSO controls (Fig. 2C,D). Kidney [^{18}F]FPA uptake is initially increased in the AZD3965 group but rapidly clears from 30 min to 120 min p.i. (Fig. 2E). This indicates that AZD3965 promotes urinary clearance of [^{18}F]FPA in mice. On the basis of observed trajectories, we identified the optimal window for cardiac imaging to be the interval from 30 to 90 min p.i..

AZD3965 reduces overall radiation absorbed dose

To supplement our image-based assessment of differential tissue radioactivity concentrations in the presence of AZD3965, we measured tissue activities at 2 h p.i. in a biodistribution experiment (Table 1). Dosimetry calculations based on these tissue activity data demonstrate that AZD3965 effectively reduces dose to all tissues (Table 1). This data was extrapolated to humans and translated to a 23% decrease in total body absorbed dose, resulting in a drop from $1.22x10^{-2}$ mSv/MBq to $9.45x10^{-3}$ mSv/MBq for males and from $1.47x10^{-2}$ mSv/MBq to $1.14x10^{-2}$ mSv/MBq for females (Table 2). These absorbed doses are comparable to those delivered to patients by [^{18}F]FDG[17]. Our calculation assumes a voiding interval of 30 min in line with literature precedent and clinical practice[18]. Longer voiding intervals lead to significantly higher absorbed doses in bladder, and consequently, higher effective doses.

Table 1

Mouse dosimetry of [^{18}F]FPA co-administered with AZD3965 or vehicle (DMSO)

30 g Male Mouse	**Tissue Activity (%ID/g)**		**Absorbed Dose (mSV/MBq) (assuming 2 h voiding interval)**		**Absorbed Dose (mSV/MBq) (assuming 30 min voiding interval**	
Target Organ	[^{18}F]FPA	[^{18}F]FPA + AZD3965	[^{18}F]FPA	[^{18}F]FPA + AZD3965	[^{18}F]FPA	[^{18}F]FPA + AZD3965
Brain	5.12 ± 0.19	1.11 ± 0.09	26.8	13.0	26.8	13.0
Large Intestine	3.75 ± 0.23	3.07 ± 0.24	13.6	11.9	13.6	11.0
Small Intestine	3.16 ± 0.21	1.92 ± 0.10	13.6	11.5	13.6	10.9
Stomach	1.77 ± 0.25	0.96 ± 0.11	14.2	11.3	14.2	11.1
Heart	3.60 ± 0.21	2.00 ± 0.25	29.8	24.0	29.8	23.9
Kidneys	3.09 ± 0.43	3.89 ± 0.44	27.4	30.5	27.4	30.2
Liver	2.70 ± 0.30	1.98 ± 0.21	21.1	14.8	21.1	14.7
Lungs	4.05 ± 0.27	1.94 ± 0.24	14.7	11.6	14.6	11.5
Pancreas	1.88 ± 0.18	1.27 ± 0.18	13.9	11.5	13.9	11.2
Skeleton	2.56 ± 0.17	2.29 ± 0.27	13.2	10.7	13.2	10.5
Spleen	3.57 ± 0.44	2.75 ± 0.31	13.2	10.9	13.2	10.7
Testes	X	X	13.2	13.1	13.2	10.6

1. Tissue activity estimated from counts in tissues collected 2 h p.i. and expressed as percent of injected dose per gram tissue (mean ± S.E.M). Tissues labeled X were not collected.

2. Residence times calculated from average activity at each time point across all animals.

3. Tissue activity at time 0 assumed to be 0 Bq/mL. For heart, initial activity assumed to be 50% ID/g, based on total mouse volume of ~ 2 mL. Mono-exponential fit used to calculate time-integrated activity between time 0 and first data point.

4. For curves where decreasing exponential was not a good model fit, (brain, bladder, AZD heart) no additional efflux assumed, only physical decay beyond last measured timepoint.

30 g Male Mouse	Tissue Activity (%ID/g)		Absorbed Dose (mSV/MBq) (assuming 2 h voiding interval)		Absorbed Dose (mSV/MBq) (assuming 30 min voiding interval	
Thyroid	X	X	13.3	10.7	13.3	10.6
Urinary Bladder	X	X	28.0	573.0	13.6	10.9
Total Body	X	X	14.1	14.2	14.0	11.0
1. Tissue activity estimated from counts in tissues collected 2 h p.i. and expressed as percent of injected dose per gram tissue (mean ± S.E.M). Tissues labeled X were not collected.						
2. Residence times calculated from average activity at each time point across all animals.						
3. Tissue activity at time 0 assumed to be 0 Bq/mL. For heart, initial activity assumed to be 50% ID/g, based on total mouse volume of ~ 2 mL. Mono-exponential fit used to calculate time-integrated activity between time 0 and first data point.						
4. For curves where decreasing exponential was not a good model fit, (brain, bladder, AZD heart) no additional efflux assumed, only physical decay beyond last measured timepoint.						

Table 2

Human radiation dosimetry of [^{18}F]FPA estimated from a mouse model

Absorbed Dose with 30 min Urinary Voiding (mSV/MBq)	**Human Male**		**Human Female**	
Target Organ	[^{18}F]FPA	[^{18}F]FPA + AZD3965	[^{18}F]FPA	[^{18}F]FPA + AZD3965
Adrenals	1.37E-02	1.08E-02	1.69E-02	1.32E-02
Brain	1.29E-02	4.29E-03	1.58E-02	5.41E-03
Breasts	N/A	N/A	1.24E-02	9.44E-03
Esophagus	1.23E-02	9.32E-03	1.24E-02	9.44E-03
Eyes	1.10E-02	7.87E-03	1.36E-02	9.58E-03
Gallbladder Wall	1.39E-02	1.04E-02	1.65E-02	1.27E-02
Left Colon	1.43E-02	1.11E-02	1.74E-02	1.36E-02
Small Intestine	1.45E-02	1.15E-02	1.62E-02	1.28E-02
Stomach Wall	1.35E-02	1.03E-02	1.66E-02	1.27E-02
Right Colon	1.41E-02	1.09E-02	1.74E-02	1.33E-02
Rectum	1.42E-02	1.22E-02	1.73E-02	1.64E-02
Heart	1.53E-02	1.18E-02	1.93E-02	1.49E-02
Kidneys	1.50E-02	1.66E-02	1.82E-02	2.01E-02
Liver	1.07E-02	6.96E-03	1.34E-02	8.76E-03
Lungs	1.19E-02	9.01E-03	1.50E-02	1.14E-02
Ovaries	N/A	N/A	1.75E-02	1.48E-02
Human TIA estimated by mass scaling of mouse TIA.				

Absorbed Dose with 30 min Urinary Voiding (mSV/MBq)	Human Male		Human Female	
Pancreas	1.44E-02	1.10E-02	1.75E-02	1.34E-02
Prostate	1.40E-02	1.27E-02	N/A	N/A
Salivary Glands	1.27E-02	9.14E-03	1.44E-02	1.04E-02
Red Marrow	1.15E-02	8.86E-03	1.40E-02	1.09E-02
Skeleton	1.24E-02	9.40E-03	1.39E-02	1.05E-02
Spleen	1.33E-02	1.03E-02	1.64E-02	1.28E-02
Testes	1.19E-02	9.52E-03	N/A	N/A
Thymus	1.24E-02	9.42E-03	1.55E-02	1.18E-02
Thyroid	1.25E-02	9.46E-03	1.42E-02	1.07E-02
Urinary Bladder	1.41E-02	4.07E-02	1.50E-02	4.61E-02
Uterus	N/A	N/A	1.73E-02	1.65E-02
Total Body	1.22E-02	9.45E-03	1.47E-02	1.14E-02
Effective Dose	1.01E-02	8.90E-03	1.38E-02	1.20E-02
Human TIA estimated by mass scaling of mouse TIA.				

[^{18}F]FPA PET imaging and tissue biodistribution correlates with doxorubicin-induced cardiotoxicity in mice

We confirmed that mice exhibited impaired cardiac function within 8 weeks of the completion of doxorubicin treatment by echocardiography (Fig. 3A). At this timepoint, these mice also exhibited lower body weights and heart weight to tibia length ratios (HW/TL) and elevated cardiac troponin-I levels (Fig. 3B-E). These outcomes are consistent with those found in studies describing doxorubicin-induced toxicity[19,20]. Another metric for assessing cardiac injury relates to the heart's propensity for using SCFA as an alternative fuel[5–7]. Cardiac abstraction and metabolism of SCFA are linked to the expression and

activities of ACSS enzymes[21,22], and these are elevated in patients and animals experiencing heart disease[6,23,24]. Therefore, we assayed the activities of ACSS enzymes in the isolated hearts of these mice as an index for increased SCFA utilization. As expected, the cardiac tissues from doxorubicin-treated animals exhibited significantly elevated levels of ACSS activities (Fig. 3F). Altogether, these indices indicate biochemical, physiological, and functional changes characteristic of doxorubicin cardiotoxicity.

We imaged these mice using [^{18}F]FPA PET and observed higher uptakes of [^{18}F]FPA in the hearts of mice treated with doxorubicin (Fig. 4). These differences were even more visually apparent in mice co-injected with AZD3965. We derived TACs from the PET images and determined that animals treated with doxorubicin sustained significantly higher ($p < 0.05$) [^{18}F]FPA signals in their hearts across all timepoints of imaging compared to their respective controls (Supplementary Fig. 1A). Moreover, these statistically significant differences were also apparent in mice co-injected with AZD3965 (Supplementary Fig. 1B). To further validate our imaging data, we performed a biodistribution study that confirmed increased [^{18}F]FPA uptake in the hearts of doxorubicin-treated mice, with the differences even more evident in the groups of mice receiving AZD3965 as a co-injection ($p < 0.05$) (Supplementary Fig. 1C). [^{18}F]FPA uptake at this timepoint was 3.60 ± 0.21%ID/g and 4.85 ± 0.25%ID/g in the untreated mice and 2.00 ± 0.25%ID/g and 4.11 ± 0.58%ID/g in the AZD3965-treated mice, respectively. Doxorubicin also increased [^{18}F]FPA uptake in many other tissues, most notably in livers, kidneys, and brains while co-injection with AZD3965 significantly reduced ($p < 0.05$) [^{18}F]FPA uptake in these off-target tissues.

Discussion

At present, the molecular imaging probes used for cardiac imaging indicate changes in myocardial perfusion[25,26], ventricular structure and function[27,28], and metabolism[29–34]. Changes in perfusion and myocardial function are associated with cardiac tissue remodeling and essentially indicate disease that is already evident by other imaging modalities[35]. By contrast, probes which report on changes in cardiac metabolism may be more suitable for detecting pre-symptomatic or sub-clinical disease as metabolic changes occur prior to the onset of cardiac injury[5,36]. Clinical cardiometabolic PET imaging is dominated by the use of [^{18}F]FDG. [^{18}F]FDG has the advantages of being readily available in most major hospitals and that its uptake in the heart correlates with some indices of cardiac dysfunction. Nevertheless, cardiac [^{18}F]FDG PET imaging is subject to the potentially confounding effect of uptake of this probe by other metabolically active cells. For example, [^{18}F]FDG, is avidly taken up by inflammatory cells and is not easily displaced from these cells. The result of this uptake pattern is decreased image sensitivity[37]. Moreover, the first step of glucose metabolism, which is shared by [^{18}F]FDG, is its phosphorylation to glucose-6-phosphate. This molecule can undergo glycolysis to afford pyruvate or enter the pentose phosphate pathway. These divergent metabolic pathways may be active to different extents in the diseased heart and may explain the reports of spatial and temporal variability of [^{18}F]FDG in hearts with cardiotoxicity[38].

Agents which report on changes in fatty acid metabolism have the potential to directly assess the energetic state of the heart due to this tissue's reliance on fatty acid oxidation for ATP. Some of the PET tracers developed for this application include [^{18}F]fluoro-6-thia-heptadecanoic acid[29,30], [^{11}C]palmitate[34], [^{11}C]acetate[31], and [^{11}C]lactate[32]. Unfortunately, their imaging applications are limited either by poor retention in the heart or catabolism by other biochemical pathways which do not correlate with the incidence of cardiac disease[29–34]. Of the many alternative substrates used by the LCFA-deficient heart, SCFA are preferentially used as they exploit the existing mechanisms for lipid catabolism[5,6]. Therefore, we hypothesized that the SCFA analog, [^{18}F]FPA, could be used as an indicator of cardiometabolic dysfunction caused by doxorubicin-induced cardiotoxicity.

We began our assessment of [^{18}F]FPA as a cardiac imaging agent by analyzing its retention in fed and fasted states. Plasma concentrations of endogenous SCFAs may be influenced by fasting as they are predominantly sourced from the gut microbiome[39]. By contrast to [^{18}F]FDG[14,40], the tissue uptake of [^{18}F]FPA is only marginally influenced by a 6 h fasting period. On this basis, we determined that fasting does not suppress cardiac uptake of [^{18}F]FPA with the consequence that it is not required before image acquisition. These findings support the practicality of this imaging probe for assessing cardiac disease.

Our experiments in healthy mice indicate that [^{18}F]FPA is taken up by nearly every tissue (Fig. 1), which we reasoned could diminish image contrast in the region of the heart and result in undesirable radiation doses to patients. Therefore, we enhanced the contrast to cardiac tissue by co-injecting [^{18}F]FPA with AZD3965, an inhibitor of MCT1[41]. We anticipated this combination would significantly reduce the uptake by non-cardiac tissues reliant on MCT1 for uptake of SCFA[7,15,16]. By contrast, SCFA freely enter cardiomyocytes without the need for these transporters[7]. The dose of AZD3965 (5 mg/kg) used to enhance cardiac image contrast may not directly translate to humans as it is several fold greater than the maximal recommended dose for patients (30 mg/70 kg)[42]. However, differences in the pharmacokinetics of this drug are apparent between humans and mice. For example, the therapeutic and subtoxic dose for mice is 100 mg/kg[43,44]. Since we suppressed background uptake of [^{18}F]FPA at 20-fold lesser concentrations of AZD3965 in mice (Fig. 2A), it may be possible to titrate this drug for use in patients to doses substantially below 30 mg.

We tested our approach in a model of doxorubicin-induced cardiotoxicity because treatment of this condition would benefit from the identification of suitable imaging biomarkers for diagnosis and monitoring response to treatment. Cardiac dysfunction caused by doxorubicin is mechanistically and pathologically distinct from more common cardiac diseases which typically lead to cardiac hypertrophy and fibrosis[35]. Therefore, relying on standard physiological and anatomical markers for diagnosis may not be effective for identifying patients at risk of developing disease. [^{18}F]FPA uptake was elevated in hearts exposed to doxorubicin and was correlated to increased activities of ACSS. This correlation suggests a mechanistic basis for the increased cardiac uptake of [^{18}F]FPA due to doxorubicin-induced cardiac injury.

Doxorubicin induces several potentially pathological changes in mice and humans, including systemic inflammation, weight loss, and cardiotoxicity[3,20]. This complex mixture of changes is likely responsible for the increased uptake of [^{18}F]FPA (Fig. 4) in blood and non-cardiac tissues. Encouragingly, co-administration of AZD3965 effectively decreased the signal due to [^{18}F]FPA in all peripheral tissues of the doxorubicin-treated mice while maintaining cardiac uptake of [^{18}F]FPA. Inflamed tissues are likely to use more SCFA as alternative substrates for metabolism or for promoting anti-inflammatory signaling cascades[45]. In this light, the ablation of doxorubicin-induced uptake of [^{18}F]FPA in blood, bones, spleens, and tails (Supplementary Fig. 1C) may reflect inhibition of its uptake by inflammatory cells, which include myeloid populations in the bone, lymphocytes in the spleens, and a combination of both in the blood. In the tails, intravenous injections may be sufficient to stimulate activation of inflammatory cells in the blood which are already primed for activation by doxorubicin[46]. Doxorubicin exposure significantly increased brain uptake of [^{18}F]FPA, but this was largely abolished by AZD3965 due to the requirement of MCT1 for permeability of SCFA through the blood brain barrier[47,48]. The term “chemobrain” is used to describe cognitive dysfunction that can arise during chemotherapy. Cognitive dysfunction is attributed to inflammatory and morphological changes which occur in the brain due to doxorubicin toxicity[49]. These events could be responsible for the increased [^{18}F]FPA uptake in the brains of these animals and suggests a possibility for using this tracer to image brain health as it is exposed to doxorubicin. Further study is needed to determine the precise mechanisms which account for all the aforementioned changes in response to doxorubicin, but our observations suggest that AZD3965 renders [^{18}F]FPA PET feasible even when systemic inflammation is present.

Interestingly, AZD3965 induces a progressive loss of cardiac signal beginning at 100 min p.i. which is not observed in the absence of the drug (Supplementary Fig. 1A). These decrements are proportionate in the hearts of both doxorubicin-treated and untreated controls (Supplementary Fig. 1B) and therefore do not invalidate our comparisons between these groups. The plasma half-life of AZD3965 is approximately 2.5 h[44]. One possible explanation for the decreasing signal is the accelerated clearance of [^{18}F]FPA from blood by AZD3965, as decrements are also evident in other highly perfused tissues (Supplementary Fig. 1C). Nevertheless, the stable cardiac signal from 30–90 min p.i. affords a broad imaging window that can be readily implemented for clinical scans.

Although we employed a well-characterized model of doxorubicin-induced cardiotoxicity for the evaluation of cardiac [^{18}F]FPA PET, we anticipate this imaging strategy may be useful in detecting other forms of cardiac injury. An early and pronounced shift in fatty acid metabolism is a common feature of all cardiac diseases[7,50]. Consequently, we plan to investigate [^{18}F]FPA as a probe for detecting incipient cardiac failure across the spectrum of heart disease, not only the disease arising from cardiotoxicity. We anticipate that our approach will also be translatable to clinical populations. Prior human studies with [^{18}F]FPA[12] and AZD3965[42] in other indications confirm their safety.

One major limitation of our study is that we investigated [^{18}F]FPA PET when cardiac dysfunction, as evidenced by decreased fractional shortening, was already evident. At this stage of disease, diagnostic imaging is possible using non-nuclear modalities and cardiac damage is irreversible. Therefore, our future work will investigate the utility of [^{18}F]FPA PET as an early indicator of doxorubicin-induced cardiotoxicity. In addition, we found, as have others, that female C57BL/6 mice are not as susceptible to doxorubicin toxicity as males[51]. Although observations in clinical populations support the hypothesis that cardiometabolic changes occur similarly in men and women, we were unable to test this hypothesis in our model.

Conclusions

We developed an optimized cardiac imaging protocol for [^{18}F]FPA PET based on the co-administration of AZD3965, an MCT1 inhibitor currently undergoing clinical evaluation, and demonstrated the suitability of this approach for imaging metabolic changes in the hearts of mice exposed to doxorubicin. As we confirmed that these mice displayed canonical features of cardiotoxicity, these results support the use of [^{18}F]FPA and AZD3965 to image doxorubicin-induced cardiotoxicity by PET. Our future studies will be focused on applying this method for imaging other cardiac diseases which are characterized by changes in fatty acid metabolism.

Declarations

Author Contributions:

Study Design: JAA, ADL, JWB, AAC, JMK.

Image and Data Acquisitions: JAA, ASW, CHL, OLM.

Image and Data Analysis: JAA, ASW, EKF, OLM.

Interpreting Results: JAA, EKF, TMJ, JMK.

Writing of Initial Manuscript: JAA, TMJ, JMK.

All authors contributed to and approved the final manuscript.

Acknowledgements:

The authors wish to acknowledge the assistance of Pradeep K. Singh, Ph.D. in the optimization of [^{18}F]FPA synthesis and the radiochemistry production team at Citigroup Biomedical Imaging Center (CBIC) at Weill Cornell Medicine for providing the fluorine-18.

Funding:

This work was partly funded by the National Cancer Institute at the National Institutes of Health (NIH) through R21CA246409-01 (awarded to J.M.K.), by the National Heart, Lung, and Blood Institute at the NIH through F32HL168948 (awarded to J.A.A.), and by the Office of The Director of the NIH under Award Number S10OD030447.

Conflicts of Interest:

The authors declare that they have no conflict of interest with regard to this study.

Ethical Approval:

This study followed all applicable institutional and/or national guidelines for the care and use of animals and approved by the Institutional Animal Care and Use Committee at Weill Cornell Medicine.

Data Availability:

All research data is available from the corresponding author upon request.

References

1. Herrmann J. Adverse cardiac effects of cancer therapies: cardiotoxicity and arrhythmia. *Nat Rev Cardiol*. 2020;17(8):474-502. doi:10.1038/s41569-020-0348-1
2. Ping Z, Peng Y, Lang H, et al. Oxidative Stress in Radiation-Induced Cardiotoxicity. *Oxid Med Cell Longev*. 2020:3579143. doi:10.1155/2020/3579143
3. Bhagat A, Kleinerman ES. Anthracycline-Induced Cardiotoxicity: Causes, Mechanisms, and Prevention. *Adv Exp Med Biol*. 2020;1257:181-192. doi:10.1007/978-3-030-43032-0_15
4. Carvalho RA, Sousa RPB, Cadete VJJ, *et al*. Metabolic remodeling associated with subchronic doxorubicin cardiomyopathy. *Toxicology*. 2010;270(2-3):92-98. doi:10.1016/J.TOX.2010.01.019
5. Lewandowski ED, Kudej RK, White LT, O'Donnell JM, Vatner SF. Mitochondrial preference for short chain fatty acid oxidation during coronary artery constriction. *Circulation*. 2002;105(3):367-372. doi:10.1161/HC0302.102594
6. Carley AN, Maurya SK, Fasano M, et al. Short-Chain Fatty Acids Outpace Ketone Oxidation in the Failing Heart. *Circulation*. 2021;143:1797-1808. doi:10.1161/CIRCULATIONAHA.120.052671
7. Palm CL, Nijholt KT, Bakker BM, Westenbrink BD. Short-Chain Fatty Acids in the Metabolism of Heart Failure – Rethinking the Fat Stigma. *Front Cardiovasc Med*. 2022;9:915102. doi:10.3389/FCVM.2022.915102
8. Pillarsetty NVK, Punzalan B, Larson SM. 2-18F-Fluoropropionic acid as a PET imaging agent for prostate cancer. *J Nucl Med*. 2009;50(10):1709-1714. doi:10.2967/JNUMED.109.064212
9. Zhang Z, Liu S, Ma H, *et al*. Validation of R-2-[18 F]Fluoropropionic Acid as a Potential Tracer for PET Imaging of Liver Cancer. *Mol imaging Biol*. 2019;21(6):1127-1137. doi:10.1007/S11307-019-01346-1

10. Zhao J, Zhang Z, Nie D, *et al*. PET Imaging of Hepatocellular Carcinomas: 18 F-Fluoropropionic Acid as a Complementary Radiotracer for 18 F-Fluorodeoxyglucose. *Mol Imaging*. 2019;18. doi:10.1177/1536012118821032
11. Zhang Z, Liu S, Tang X, *et al*. Radiosynthesis and preliminary biological evaluation of the 2-[18F]fluoropropionic acid enantiomers for tumor PET imaging. *J Radioanal Nucl Chem*. 2018;316(1):153-159. doi:10.1007/S10967-018-5753-0
12. Zhang Z, Liu S, Ma H, *et al*. Propionic Acid-Based PET Imaging of Prostate Cancer. *Mol Imaging Biol*. 2021;23(6):836-845. doi:10.1007/S11307-021-01608-X
13. De Martino M, Daviaud C, Minns HE, *et al*. Radiation therapy promotes unsaturated fatty acids to maintain survival of glioblastoma. *Cancer Lett*. 2023;570:216329. doi:10.1016/J.CANLET.2023.216329
14. Surasi DS, Bhambhvani P, Baldwin JA, Almodovar SE, O'Malley JP. 18F-FDG PET and PET/CT Patient Preparation: A Review of the Literature. *J Nucl Med Technol*. 2014;42(1):5-13. doi:10.2967/JNMT.113.132621
15. Kamp F, Hamilton JA. How fatty acids of different chain length enter and leave cells by free diffusion. *Prostaglandins Leukot Essent Fat Acids*. 2006;75(3):149-159. doi:10.1016/j.plefa.2006.05.003
16. Kirat D, Masuoka J, Hayashi H, *et al*. Monocarboxylate transporter 1 (MCT1) plays a direct role in short-chain fatty acids absorption in caprine rumen. *J Physiol*. 2006;576(Pt 2):635. doi:10.1113/JPHYSIOL.2006.115931
17. Srinivasan S, Crandall JP, Gajwani P, *et al*. Human Radiation Dosimetry for Orally and Intravenously Administered 18F-FDG. *J Nucl Med*. 2020;61(4):613-619. doi:10.2967/JNUMED.119.233288
18. Gnesin S, Cicone F, Mitsakis P, *et al*. First in-human radiation dosimetry of the gastrin-releasing peptide (GRP) receptor antagonist 68 Ga-NODAGA-MJ9. *EJNMMIRes*. 2018;8(1):1-10. doi:10.1186/S13550-018-0462-9/FIGURES/4
19. Mitry MA, Edwards JG. Doxorubicin induced heart failure: Phenotype and molecular mechanisms. *IJC Hear Vasc*. 2016;10:17-24. doi:10.1016/J.IJCHA.2015.11.004
20. Podyacheva EY, Kushnareva EA, Karpov AA, Toropova YG. Analysis of models of doxorubicin-induced cardiomyopathy in rats and mice. A modern view from the perspective of the pathophysiologist and the clinician. *Front Pharmacol*. 2021;12:670479. doi:10.3389/FPHAR.2021.670479/FULL
21. Hele P. The acetate activating enzyme of beef heart. *J Biol Chem*. 1954;206(2):671-676. doi: 10.1016/S0021-9258(19)50835-3
22. Groot PH. The activation of short-chain fatty acids by the soluble fraction of guinea-pig heart and liver mitochondria. The search for a distinct propionyl-CoA synthetase. *Biochim Biophys Acta*. 1975;380(1):12-20. doi:10.1016/0005-2760(75)90040-5
23. Tanno M, Kuno A, Horio Y, Miura T. Emerging beneficial roles of sirtuins in heart failure. *Basic Res Cardiol*. 2012;107(4). doi:10.1007/S00395-012-0273-5

24. Colak D, Kaya N, Al-Zahrani J, *et al*. Left ventricular global transcriptional profiling in human end-stage dilated cardiomyopathy. *Genomics*. 2009;94(1):20. doi:10.1016/J.YGENO.2009.03.003
25. Laursen AH, Elming MB, Ripa RS, *et al*. Rubidium-82 positron emission tomography for detection of acute doxorubicin-induced cardiac effects in lymphoma patients. *J Nucl Cardiol*. 2020;27(5):1698-1707. doi:10.1007/S12350-018-1458-6
26. Nehmeh SA, Fox JJ, Schwartz J, *et al*. A pilot study of 13N-ammonia cardiac PET imaging to assess subacute cardiotoxicity following adjuvant intensity-modulated radiotherapy for locally advanced breast cancer. *Clin Imaging*. 2020;68:283-290. doi:10.1016/J.CLINIMAG.2020.07.026
27. Marzlin N, Hays AG, Peters M, *et al*. Myocardial Work in Echocardiography. *Circ Cardiovasc Imaging*. 2023;16(2):E014419. doi:10.1161/CIRCIMAGING.122.014419
28. Santini F, Gui L, Lorton O, *et al*. Ultrasound-driven cardiac MRI. *Phys Medica*. 2020;70:161-168. doi:10.1016/J.EJMP.2020.01.008
29. Taylor M, Wallhaus TR, Degrado TR, *et al*. An evaluation of myocardial fatty acid and glucose uptake using PET with [18F]fluoro-6-thia-heptadecanoic acid and [18F]FDG in Patients with Congestive Heart Failure. *J Nucl Med*. 2001;42(1):55-62.
30. Takala TO, Nuutila P, Pulkki K, *et al*. 14(R,S)-[18F]Fluoro-6-thia-heptadecanoic acid as a tracer of free fatty acid uptake and oxidation in myocardium and skeletal muscle. *Eur J Nucl Med*. 2002;29(12):1617-1622. doi:10.1007/s00259-002-0979-y
31. Armbrecht JJ, Buxton DB, Brunken RC, Phelps ME, Schelbert HR. Regional myocardial oxygen consumption determined noninvasively in humans with [1-11C]acetate and dynamic positron tomography. *Circulation*. 1989;80(4):863-872. doi:10.1161/01.CIR.80.4.863
32. Herrero P, Dence CS, Coggan AR, Kisrieva-Ware Z, Eisenbeis P, Gropler RJ. L-3-11C-lactate as a PET tracer of myocardial lactate metabolism: a feasibility study. *J Nucl Med*. 2007;48(12):2046-2055. doi:10.2967/JNUMED.107.044503
33. Kelly JM, Babich JW. PET Tracers for Imaging Cardiac Function in Cardio-oncology. *Curr Cardiol Rep*. 2022;24(3):247. doi:10.1007/S11886-022-01641-4
34. Sobel BE, Weiss ES, Welch MJ, Siegel BA, Ter-Pogossian MM. Detection of remote myocardial infarction in patients with positron emission transaxial tomography and intravenous 11C-palmitate. *Circulation*. 1977;55(6):853-857. doi:10.1161/01.CIR.55.6.853
35. Kemp CD, Conte J V. The pathophysiology of heart failure. *Cardiovasc Pathol*. 2012;21(5):365-371. doi:10.1016/J.CARPATH.2011.11.007
36. Doenst T, Nguyen TD, Abel ED. Cardiac Metabolism in Heart Failure. *Circ Res*. 2013;113(6):709-724. doi:10.1161/CIRCRESAHA.113.300376
37. Krishnaraju VS, Singh H, Kumar R, Sharma S, Mittal BR, Bhattacharya A. Infection imaging using [18F]FDG-labelled white blood cell positron emission tomography–computed tomography. *Br J Radiol*. 2021;94(1122). doi:10.1259/BJR.20201204
38. Bauckneht M, Cossu V, Miceli A, *et al*. FDG-PET Imaging of Doxorubicin-Induced Cardiotoxicity: a New Window on an Old Problem. *Curr Cardiovasc Imaging Rep*. 2019;12(11):1-8.

doi:10.1007/S12410-019-9517-1/FIGURES/3

39. Cummings JH, Pomare EW, Branch WJ, Naylor CP, Macfarlane GT. Short chain fatty acids in human large intestine, portal, hepatic and venous blood. *Gut*. 1987;28(10):1221-1227. doi:10.1136/GUT.28.10.1221
40. Tang R, Wang JTY, Wang L, *et al*. Impact of Patient Preparation on the Diagnostic Performance of 18F-FDG PET in Cardiac Sarcoidosis: A Systematic Review and Meta-analysis. *Clin Nucl Med*. 2016;41(7):e327-e339. doi:10.1097/RLU.0000000000001063
41. Bola BM, Chadwick AL, Michopoulos F, *et al*. Inhibition of monocarboxylate transporter-1 (MCT1) by AZD3965 enhances radiosensitivity by reducing lactate transport. *Mol Cancer Ther*. 2014;13(12):2805-2816. doi:10.1158/1535-7163.MCT-13-1091
42. Halford S, Veal GJ, Wedge SR, *et al*. A Phase I Dose-Escalation Study of AZD3965, an Oral Monocarboxylate Transporter 1 Inhibitor, in Patients with Advanced Cancer. *Clin Cancer Res*. 2023;29(8):1429-1439.doi:10.1158/1078-0432.CCR-22-2263.
43. Benyahia Z, Blackman MCNM, Hamelin L, *et al*. In Vitro and In Vivo Characterization of MCT1 Inhibitor AZD3965 Confirms Preclinical Safety Compatible with Breast Cancer Treatment. *Cancers (Basel)*. 2021;13(3):1-25. doi:10.3390/CANCERS13030569
44. Guan X, Morris ME. Pharmacokinetics of the Monocarboxylate Transporter 1 Inhibitor AZD3965 in Mice: Potential Enterohepatic Circulation and Target-Mediated Disposition. *Pharm Res*. 2020;37(1):1-13. doi:10.1007/S11095-019-2735-Z/TABLES/3
45. Den Besten G, Van Eunen K, Groen AK, Venema K, Reijngoud DJ, Bakker BB. The role of short-chain fatty acids in the interplay between diet, gut microbiota, and host energy metabolism. *J Lipid Res*. 2013;54(9):2325-2340. doi:10.1194/JLR.R036012
46. Wang L, Chen Q, Qi H, *et al*. Doxorubicin-induced systemic inflammation is driven by upregulation of toll-like receptor TLR4 and endotoxin leakage. *Cancer Res*. 2016;76(22):6631-6642. doi: 10.1158/0008-5472.CAN-15-3034
47. Bergersen L, Rafiki A, Ottersen OP. Immunogold cytochemistry identifies specialized membrane domains for monocarboxylate transport in the central nervous system. *Neurochem Res*. 2002;27(1-2):89-96. doi:10.1023/A:1014806723147
48. Pierre K, Pellerin L, Debernardi R, Riederer BM, Magistretti PJ. Cell-specific localization of monocarboxylate transporters, MCT1 and MCT2, in the adult mouse brain revealed by double immunohistochemical labeling and confocal microscopy. *Neuroscience*. 2000;100(3):617-627. doi:10.1016/S0306-4522(00)00294-3
49. Cardoso CV, de Barros MP, Bachi AL, *et al*. Chemobrain in rats: Behavioral, morphological, oxidative and inflammatory effects of doxorubicin administration. *Behav Brain Res*. 2020;378. doi:10.1016/J.BBR.2019.112233
50. Osorio JC, Stanley WC, Linke A, *et al*. Impaired myocardial fatty acid oxidation and reduced protein expression of retinoid X receptor-α in pacing-induced heart failure. *Circulation*. 2002;106(5):606-612. doi:10.1161/01.CIR.0000023531.22727.C1

51. Agostinucci K, Grant MKO, Melaku W, Nair C, Zordoky BN. Exposure to Doxorubicin Modulates the Cardiac Response to Isoproterenol in Male and Female Mice. *Pharmaceuticals*. 2023;16(3). doi:10.3390/PH16030391

Figures

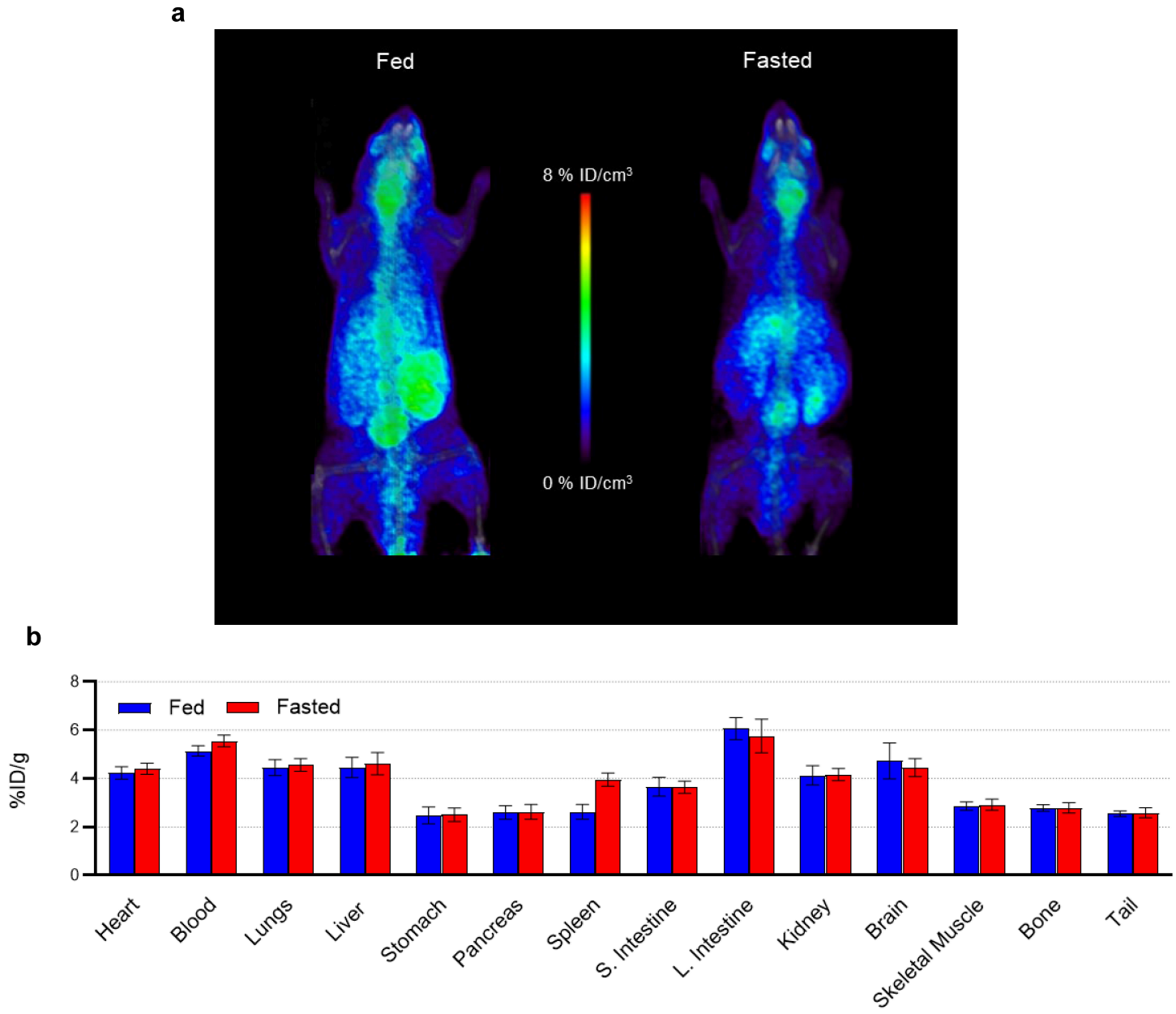

Figure 1

[^{18}F]FPA PET/CT Imaging and Tissue Biodistribution of Fed and Fasted Mice. **(a)** Sixty-minute dynamic acquisitions were performed 60 min p.i. of 9.25-11.1 MBq in fed mice, and mice fasted for 6 h. These

animals were euthanized, and their tissues excised 120 min p.i. **(b)** Tissue uptake was determined as a percent of injected dose per gram tissue (%ID/g) (mean ± S.E.M.; n = 4 *p < 0.05, two-way ANOVA, Šídák post hoc).

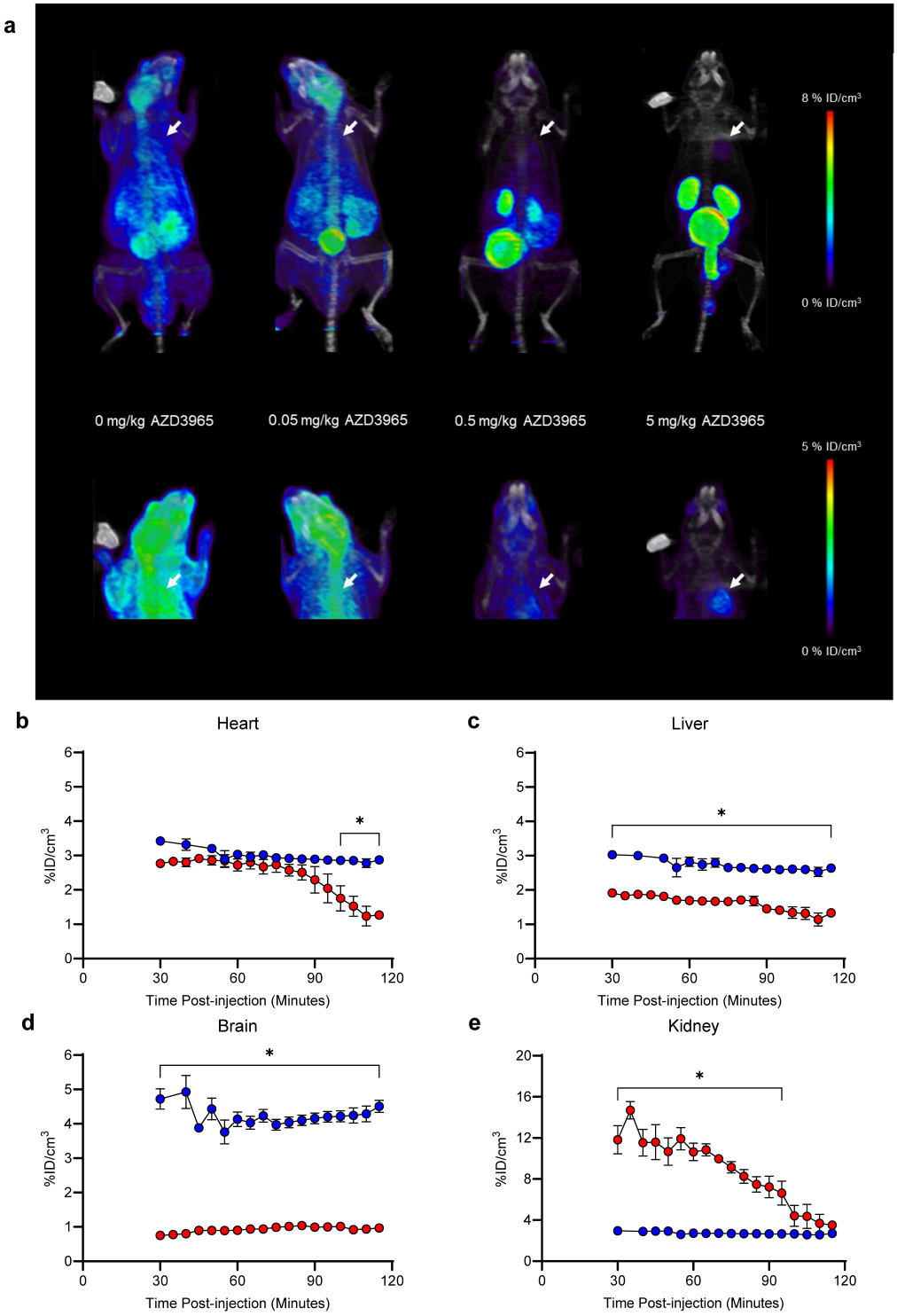

Figure 2

Dose Titration of AZD3965 for [^{18}F]FPA PET/CT Cardiac Imaging. **(a)** Increasing concentrations of AZD3965 (0, 0.05, 0.5, 5 mg/kg) were co-injected with 9.25-11.1 MBq (250-300 µCi) of [^{18}F]FPA. The

mice were imaged for 60 min by PET/CT starting at 60 min p.i. (n = 4). Hearts are indicated by white arrows. Time activity curves for **(b)** hearts, **(c)** livers, **(d)** brains, and **(e)** kidneys taken from image-based quantitation of sixty-minute dynamic PET acquisitions (12 x 5 min frames) starting at 20- and 60-min p.i. are shown. Kinetic differences between animals co-injected with AZD3965 or vehicle (DMSO) are illustrated (mean ± S.E.M.; n = 9-11; *p < 0.05, two-way ANOVA, Šídák post hoc).

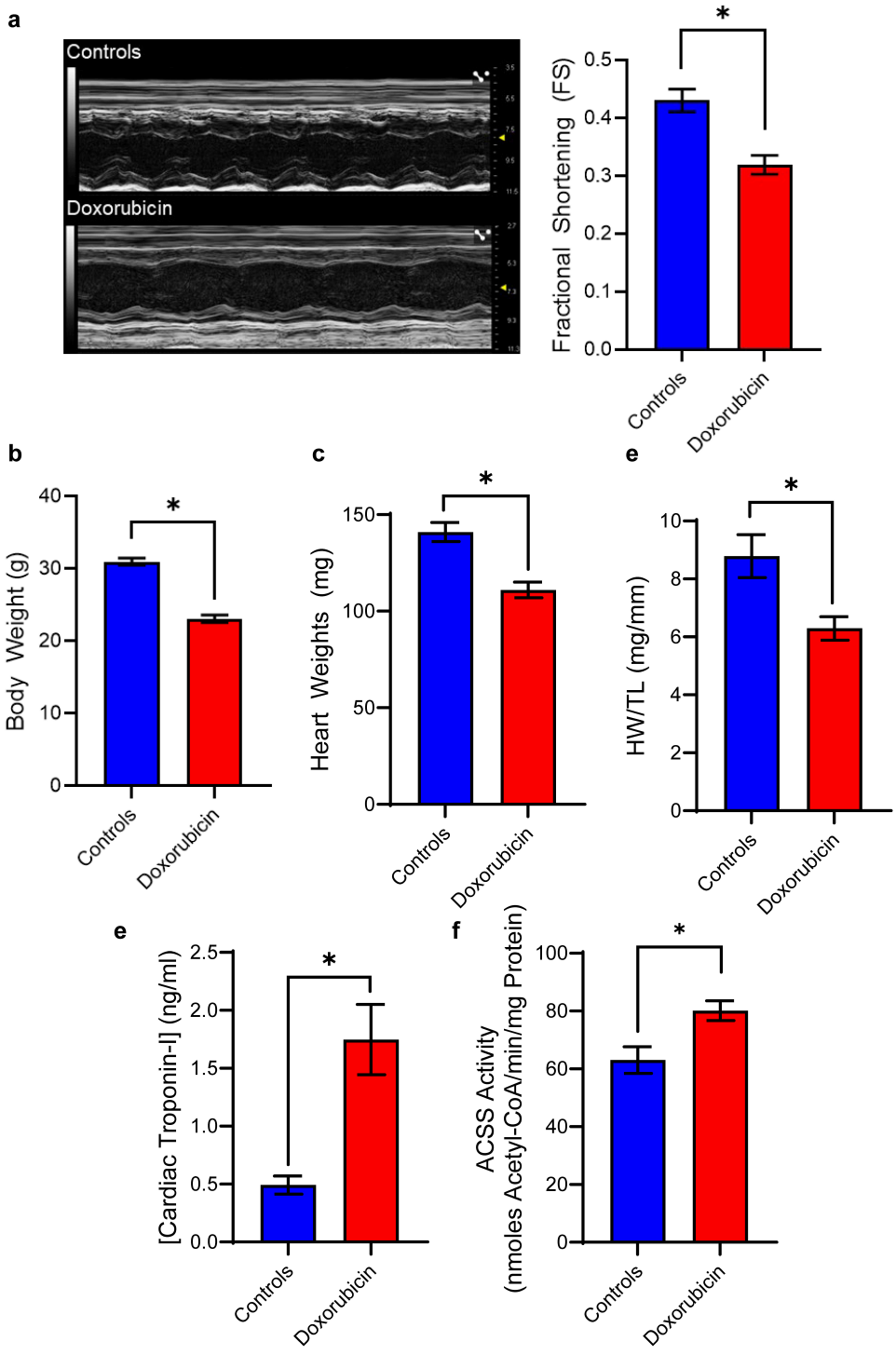

Figure 3

Indicators of Pathology in Mouse Model of Doxorubicin-induced Cardiotoxicity. **(a)** Doxorubicin-induced cardiac dysfunction was determined by decreased fractional shortening ratios acquired from echocardiograms. (mean ± S.E.M.; n = 4-8, *p < 0.05, independent t-test). **(b)** Mice (mean ± S.E.M.; n = 14, *p < .05, independent t-test) and **(c)** hearts (mean ± S.E.M.; n = 14, *p < .05, independent t-test) were weighed post-mortem. **(d)** Tibia lengths were also measured to generate heart weight to tibia length ratios (HW/TL) (mean ± S.E.M.; n = 3-6, *p < .05, independent t-test). **(e)** Serum cardiac troponin-I concentrations were determined by ELISA (mean ± S.E.M.; n = 8-10, *p < .05, independent t-test) **(f)** Acyl-CoA synthetase short-chain family (ACSS) activity was determined by evolution of pyrophosphate by product in heart homogenates (mean ± S.E.M.; n = 9, *p < .05, independent t-test).

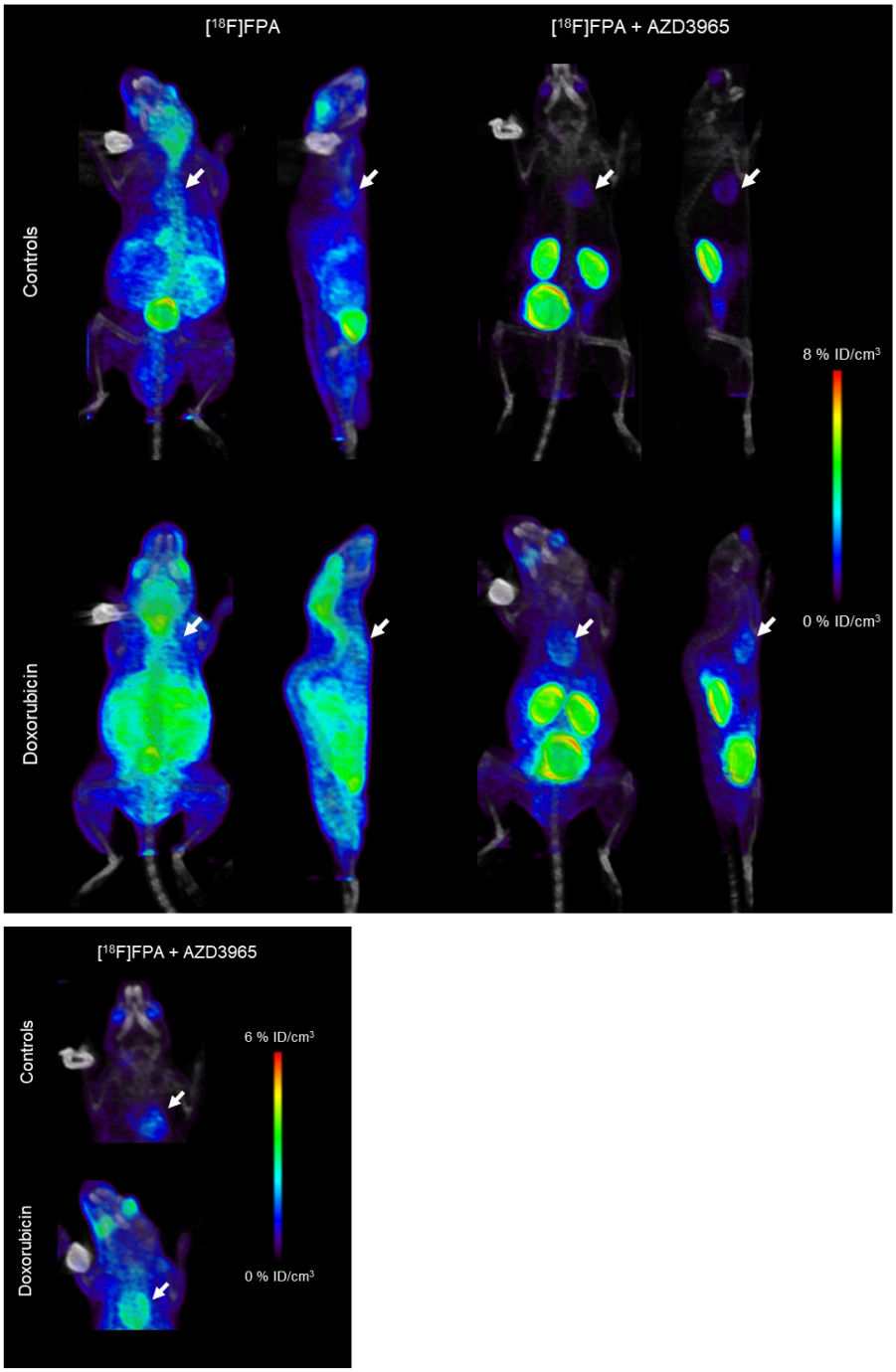

Figure 4

[^{18}F]FPA PET/CT Imaging of Doxorubicin-induced Cardiotoxicity. Mice were injected with 9.25-11.1 MBq of [^{18}F]FPA and sixty-minute dynamic PET acquisitions (12 x 5 min frames) were performed 60 minutes p.i.. [^{18}F]FPA PET/CT (coronal and sagittal images) of doxorubicin-treated and control mice co-injected with or without 5 mg/kg AZD3965 are shown. Hearts are indicated by white arrows on figures.

Supplementary Files

This is a list of supplementary files associated with this preprint. Click to download.

- ElectronicSupportingMaterial.pdf
- SupplementaryFigure1.jpg